Letter

# Photoinduced strange metal with electron and hole quasiparticles

Nagamalleswararao Dasari,[1,*] Jiajun Li,[1] Philipp Werner,[2] and Martin Eckstein[1,†]
[1]*Department of Physics, University of Erlangen-Nuremberg, 91058 Erlangen, Germany*
[2]*Department of Physics, University of Fribourg, 1700 Fribourg, Switzerland*

(Received 12 October 2020; revised 14 April 2021; accepted 10 May 2021; published 21 May 2021)

Photodoping of Mott insulators or correlated metals can create an unusual metallic state which simultaneously hosts holelike and electronlike particles. We study the dynamics of this state up to long times, as it passes its kinetic energy to the environment. When the system cools down, it crosses over from a bad metal into a resilient quasiparticle regime, in which quasiparticle bands are formed with separate Fermi levels for electrons and holes, but quasiparticles do not yet satisfy the Fermi-liquid paradigm. Subsequently, the transfer of energy to the environment slows down significantly, and the system does not reach the Fermi-liquid state even on the timescale of picoseconds. The transient photodoped strange metal exhibits unusual properties of relevance for ultrafast charge and heat transport: In particular, there can be an asymmetry in the properties of electrons and holes, and strong correlations between electrons and holes, as seen in the spectral properties.

DOI: 10.1103/PhysRevB.103.L201116

*Introduction.* Ultrafast laser excitation provides a new avenue for manipulating correlated quantum states in condensed matter [1,2], and has led to intriguing observations such as light-induced superconductivity and metastable hidden phases [3–6]. An interesting direction in this context is the optical manipulation of Mott insulators (MIs), which are the parent compound for a variety of complex states [7]. Because chemical doping leads to correlated metallic, pseudogap and superconducting phases, photodoping, i.e., an optical excitation which simultaneously generates electronlike and holelike carriers, has early on been identified as a potential route for materials control [8–16]. A short pulse can almost instantly transform the MI into a hot metallic state. The presence of carriers is demonstrated by a Drude peak in the conductivity and, because a large Mott gap prevents a rapid carrier recombination through electron-spin, electron-phonon, or electron-electron scattering [17–22], these carriers can last up to picoseconds. On this timescale, the energy transfer to the environment may then establish a *cold photodoped state* before recombination of the photocarriers. More generally, applying the same protocol to an already doped MI will generate a strange metal with unequal densities of electronlike and holelike carriers. The properties of such a correlated liquid, and in particular how they differ from the chemically doped state, remain an intriguing question.

For very large photodoping, e.g., $\eta$-pairing superconductivity has been predicted [23–25], but already the normal state properties pose fundamental questions, as doped MIs are often strange metals with non-Fermi-liquid properties [26–34]. For example, quasiparticle excitations can be observed at temperatures well above the range of validity of Fermi-liquid theory, $T_{\mathrm{FL}}$, before they disappear in the bad metallic regime around $T_{\mathrm{MIR}}$ [26]. Such resilient quasiparticle excitations dominate the transport properties of doped MIs in the intermediate temperature regime $T_{\mathrm{FL}} \lesssim T \lesssim T_{\mathrm{MIR}}$. Out of equilibrium, additional fundamental questions arise: Can there be a Fermi liquid at all with both electron and hole quasiparticles at *different* Fermi energies? In principle, such a two-species Fermi liquid is possible if the number of each species is separately conserved. In the present case, however, this conservation is only valid up to a given timescale, while the time for the formation of a Fermi liquid is at least beyond the range of previous numerical simulations [35,36]. Another interesting question concerns the particle-hole asymmetry: If the initial state is already doped from the outset, photoexcitation will lead to a photodoped state with an imbalance in the electron and hole doping. As properties of carriers in a doped Mott insulator strongly depend on the doping level, these two types of carriers could exhibit different properties. If so, this should not only influence the charge transport properties, but also the rather little explored question of thermoelectric properties on the ultrafast timescale.

While dynamical mean-field theory (DMFT) [37] is, in principle, ideally suited to study the Mott phase, previous simulations simply could not reach sufficiently long times to systematically examine the cold photodoped states [24,35,36]. Here we use a systematic and convergent truncation of the Kadanoff-Baym equations within DMFT to reach about 50-times-longer simulation times [38–40]. This allows us to study the properties of the photodoped MI up to thousands of hopping times, corresponding to a picosecond timescale if the bandwidth is in the eV range.

*Model and method.* We simulate the relaxation dynamics of doped Mott insulators by considering the single-band Hubbard model,

$$\mathcal{H} = -J \sum_{\langle ij\rangle,\sigma} c^{\dagger}_{i\sigma} c_{j\sigma} + U \sum_{i} n_{i\uparrow} n_{i\downarrow} - \mu \sum_{i\sigma} n_{i\sigma}. \quad (1)$$

*nagamalleswararao.d@gmail.com
†martin.eckstein@fau.de

 

The first term in the above Hamiltonian represents the electron hopping between nearest-neighbor lattice sites, and the second term is the on-site Coulomb interaction between electrons of opposite spin. The chemical potential $\mu$ fixes the total number of particles. In equilibrium, the system is a Mott insulator at half filling $n = \langle n_{i\uparrow} + n_{i\downarrow} \rangle = 1$ and $U \gg J$, and turns into a strongly correlated metallic state upon doping. Without loss of generality, we focus on states which are initially half filled or electron doped, where $\delta = n - 1$ quantifies the initial chemical doping. We solve the Hubbard model on a Bethe lattice using nonequilibrium dynamical mean-field theory [41]. The interacting local Green's function $G(t, t')$ is obtained by solving the auxiliary quantum impurity problem on the L-shaped Kadanoff-Baym contour using the noncrossing approximation [42]. In our calculations, we fix the hopping energy scale $J = 1$, so that the bare bandwidth is $W = 4J$. Furthermore, we set $\hbar = 1$ and measure time in units of $\hbar/J$. Unless otherwise stated, we fix the Hubbard interaction to $U = 8$. In addition to the Hamiltonian (1), a thermal bath is coupled to each site to simulate the energy dissipation from the electrons to other degrees of freedom [35]. The bath is incorporated diagrammatically with a self-energy $\Delta_{\text{bath}}(t, t') = \lambda G(t, t') D_{\text{bath}}(t, t')$, which corresponds to a Holstein-type coupling of strength $\lambda$ to a bath of bosonic degrees of freedom at given temperature $T_f$ and a linear (Ohmic) density of states, $D_{\text{bath}}(\omega) = \frac{\omega}{\omega_c} e^{-\omega/\omega_c}$, up to a cutoff energy $\omega_c = 0.2$. $D_{\text{bath}}(t, t')$ is the corresponding bath propagator. The DMFT equations are analogous to Ref. [35], but they are solved using a convergent truncation of the memory integrals in the Kadanoff-Baym equations (see Supplemental Material [43]).

*Setting.* We initially prepare an electron-doped system of filling $n = 1 + \delta$ at a very high temperature $T_i = 2$ (in the bad metal regime), and couple it to a heat bath at lower temperature $T_f = 0.05$ for times $t > 0$. This protocol serves to generate simultaneous hole and electron doping (see below) through thermal excitation $T_i$ rather than through photoexcitation. We nevertheless refer to the transient state as *photodoped* because we focus on its long-time behavior, while details of different carrier generation protocols quickly become irrelevant [35,44]. We have confirmed this using a short laser pulse and discuss the results in the Supplemental Material [43]. The system can be characterized by the time-dependent single-particle spectral function $A(t, \omega) = -\frac{1}{\pi} \text{Im} \int_0^{t_{\max}} ds\, G^R(t, t - s) e^{-i\omega s}$ and the corresponding occupied density of states $A^<(t, \omega) = -\frac{1}{\pi} \text{Im} \int_0^{t_{\max}} ds G^<(t, t - s) e^{-i\omega s}$ and unoccupied density of states $A^>(t, \omega) = A(t, \omega) - A^<(t, \omega)$; see Fig. 1(d). The spectra feature well-separated upper and lower bands, so that a time-dependent electron- and hole-doping value can be obtained from the integrated occupied density of states in the upper band, $n_e(t) = \int_{\text{UHB}} d\omega A^<(\omega, t)$, and the integrated unoccupied density of states in the lower band, $n_h(t) = \int_{\text{LHB}} d\omega A^>(\omega, t)$, respectively. In a low-temperature equilibrium state, $n_h(t) = 0$ and $n_e(t) = \delta$, but in the transient state, the system has both hole doping $n_h > 0$ and electron doping $n_e > \delta$, with $n_h = n_e - \delta$ of the order of a few percent.

*Results.* A first picture of the formation of a cold photodoped state is given by the behavior of the photodoping level and the kinetic energy. The decay of the photodoping, $n_h(t) = n_e(t) - \delta > 0$, due to carrier recombination is slow

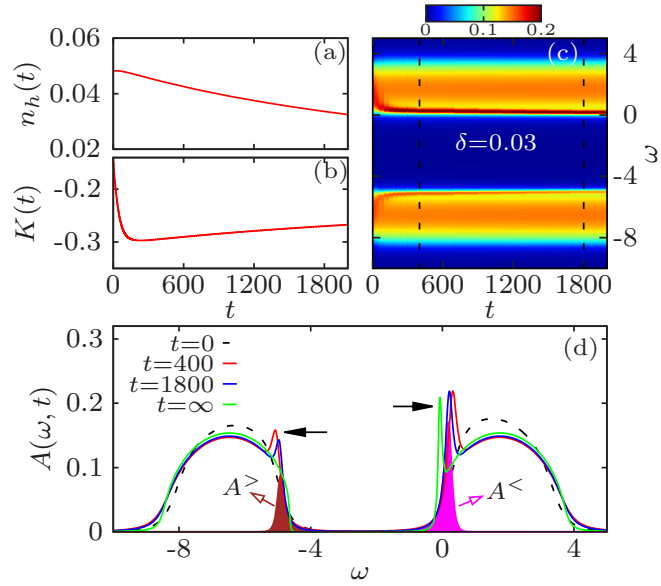


FIG. 1. Dynamics of the photodoped state at $\delta = 0.03$. (a) Photodoping level $n_h(t)$. (b) Kinetic energy $K(t)$. (c) Intensity map of the single-particle spectral function $A(\omega, t)$. (d) Line cuts of (c), showing the spectral function at selected times. Black arrows indicate the electron and hole quasiparticle states in the spectral function. The shaded area labeled with $A^>$ and $A^<$ shows the unoccupied (occupied) density of states in the lower (upper) Hubbard band at time $t = 1800$.

for all times, as expected for $U \gg J$ and a large Mott gap [Fig. 1(a)]. The kinetic energy instead drops quickly at early times, as energy is transferred from the electrons to the bath and the cold photodoped state is formed, and then follows the slow dynamics of the carrier recombination [Fig. 1(b)]. The spectral function [Figs. 1(c) and 1(d)] shows just two bands of incoherent excitations above and below the Mott gap immediately after the temperature quench. Within a few-hundred hopping times, a narrow band emerges at the upper edge of the Mott gap, which is reminiscent of the quasiparticle band of the electron-doped Mott insulator in equilibrium. At the same time, a similar (smaller) hole quasiparticle band emerges at the lower edge of the Mott gap. We emphasize that these quasiparticle bands emerge as a consequence of (photo)doping, and are therefore different from the fine structure at the edge of the Hubbard bands, which can be seen in equilibrium at half filling closer to the metal-insulator transition [45]. At late times, these quasiparticle peaks slowly evolve, which is a consequence of the reduction of the effective temperature (see discussion below) and the decay of the photodoping. The behavior is qualitatively the same for different values of the electron-phonon coupling $\lambda$ (the results are for $\lambda = 0.5$ unless otherwise stated). Previous DMFT simulations of photodoped Mott insulators [35] could only observe the onset of the formation of these quasiparticle bands, and have mostly focused on the half-filled case. With the long-time simulations, we can now address in more detail the relaxation behavior and the spectral properties of the state. We first analyze these properties at the latest time ($t = 2000$), before discussing the relaxation dynamics.

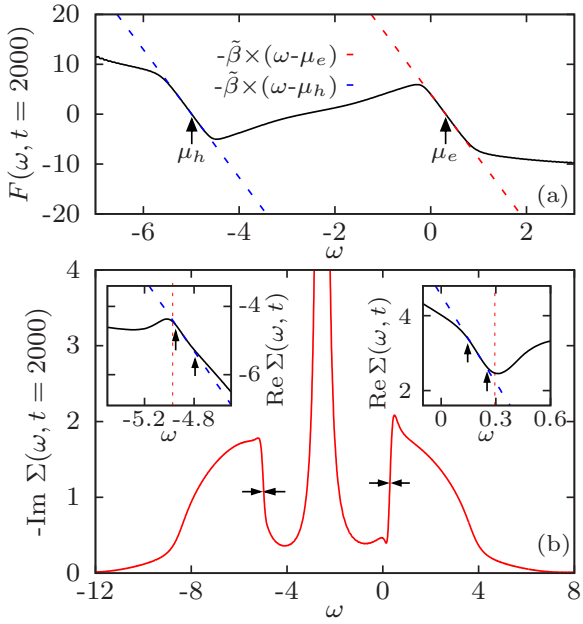


FIG. 2. Distribution function and self-energy of the transient state for $\delta = 0.03$. (a) $F(\omega, t)$ at $t = 2000$. Dashed lines show linear fits around the location of the electron and hole quasiparticle peaks. Vertical arrows indicate the electron and hole Fermi levels. (b) Imaginary part of the self-energy in the transient state at $t = 2000$. The horizontal arrows indicate the electron and hole Fermi levels. Insets: Real part of the self-energy near the electron and hole Fermi levels (red dashed lines). Blue dashed lines show the linear fit to the real part of the self-energy. The vertical arrows indicate the energies where the deviations from the linear behavior occur.

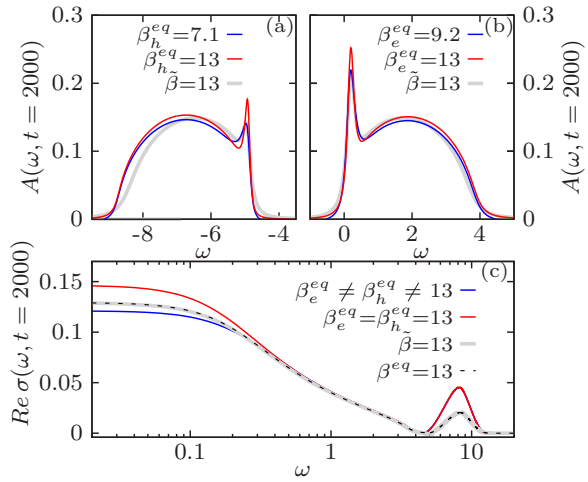


FIG. 3. Comparison between the photodoped state at $\delta = 0.03$ and $t = 2000$, where $n_e = 0.062$ and $n_h = 0.032$, and chemically doped states: (a) Lower Hubbard band of the photodoped state (light gray) and for an equilibrium system with filling $n = 1 - n_h$, at $\beta = 13$ (same temperature $1/\tilde{\beta}$ as the photodoped state) and $\beta = 7.1$. (b) Comparison of the upper Hubbard band to electron-doped systems. (c) Optical conductivity $\sigma(\omega)$ of the transient state (bold light-gray), of an equilibrium system with filling $n = 1 + n_h + n_e$ and $\beta = 13$ (black dashed line), and sum of the conductivities of systems with $n = 1 - n_h$ and $n = 1 + n_e$ (solid blue and red lines). For the solid blue line, the equilibrium inverse temperature in the electron-doped state $\beta_e^{\mathrm{eq}}$ is set to 9.2, while for the hole-doped state, $\beta_h^{\mathrm{eq}}$ is set to 7.1.

The nature of the transient state is further explored by looking at the distribution function $f(\omega, t) = A^<(\omega, t)/A(\omega, t)$. In an equilibrium state, $f(\omega)$ is just the Fermi function. It is therefore convenient to analyze the function $F(\omega, t) = \ln[A^<(\omega, t)/A^>(\omega, t)]$, which becomes $F(\omega) = -\tilde{\beta}(\omega - \tilde{\mu})$ if the system is in a quasithermal state in which the distribution is given by a Fermi function with inverse temperature $\tilde{\beta}$ and Fermi level $\tilde{\mu}$. In the transient state, $F(\omega, t)$ has such a linear behavior in the frequency range of the electron and hole quasiparticle peaks [Fig. 2(a)]. In the remaining frequency range, either the spectral weight is small (gap) or the occupation is close to zero or one. The distribution function therefore shows that the photodoped Mott insulator at long times is well described by two separately thermalized subsystems of electronlike and holelike quasiparticles. From the linear fit of $F(\omega, t)$ to $-\tilde{\beta}_{e,h}(\omega - \mu_{e,h})$, we can extract the inverse effective temperature $\tilde{\beta}$, which turns out to be approximately the same for electrons and holes, and the separate Fermi levels $\mu_e$ and $\mu_h$ of these degrees of freedom [arrows in Fig. 2(a)].

At zero temperature, the Fermi surface separates occupied energy states from unoccupied states with a step function [46]. In the present case, this step is broadened, and whether the electron and hole liquids can be considered as a Fermi liquid must be answered by the spectral properties, in particular the self-energy. In a Fermi liquid, the scattering rate of the dressed quasiparticles near the Fermi surface is determined by the single-particle self-energy $\gamma(\omega) = -\,\mathrm{Im}\,\Sigma(\omega) \sim C\omega^2 + C'T^2$ [47]. We therefore analyze the self-energy around the positions $\mu_{h,e}$ of the electron and hole quasiparticle peaks in the spectral function [Fig. 2(b)]; $\Sigma(t, \omega)$ is obtained from the Dyson equation, $\Sigma(t, \omega) = G_0(t, \omega)^{-1} - G(t, \omega)^{-1}$. At the Fermi levels, $\gamma(\omega, t)$ has a linear behavior rather than a quadratic form, which indicates that the transient state does not belong to the Fermi-liquid regime, although quasiparticle peaks are well defined in the spectral function. This is reminiscent of the resilient quasiparticle regime [26] in equilibrium. The real part $\mathrm{Re}\,\Sigma(\omega, t)$ of the self-energy shows a linear behavior around the quasiparticle peaks, which, however, does not extend up to the Fermi levels. Deviations from the linear behavior are observed at two distinct energy scales; see vertical arrows in Fig. 2(b). The change in the slope of the linear behavior should lead to the appearance of characteristic "kinks" in the quasiparticle dispersion [48].

To further understand the nature of the photodoped state and, in particular, the origin of the resilient quasiparticles, we next compare the transient state with chemically doped states. In Fig. 3(a), we compare the lower Hubbard bands with the hole quasiparticle peak in the photodoped state with hole-doping level $n_h$ to the corresponding equilibrium spectrum in a purely hole-doped system with filling $n = 1 - n_h$. Interestingly, if the temperature $T$ of the equilibrium system is chosen equal to the temperature of the photodoped system ($1/T = \tilde{\beta} = 13$), the quasiparticle peak is overestimated. This can be explained by the fact that the presence of electronlike quasiparticles in the photodoped state provides an additional scattering channel which drives the holes farther

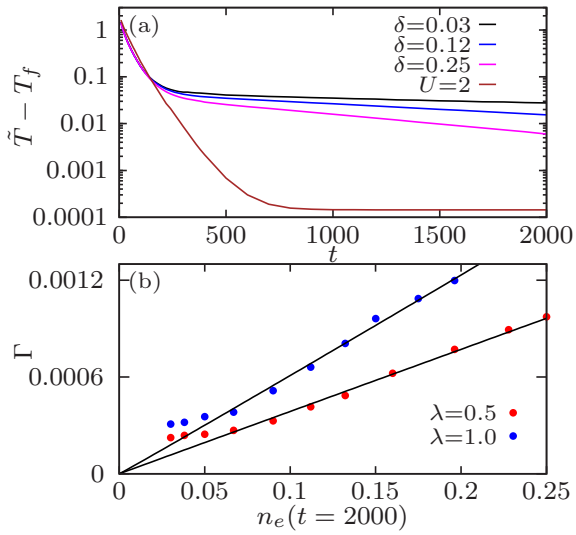


FIG. 4. (a) Difference of the effective temperature $\tilde{T} = 1/\tilde{\beta}$, obtained from fits like in Fig. 2(a) at different times, and the bath temperature $T_f = 0.05$, as a function of $t$ for different values of $\delta$. (b) Exponential decay rate of $\tilde{T} - T_f$ obtained from the curves in (a) at $t = 2000$, plotted against the photodoping $n_e(t)$ at the same time.

from the Fermi-liquid regime into a resilient quasiparticle regime. Heuristically, this is confirmed by the observation that the quasiparticle peak of the transient state can be more accurately reproduced when a higher temperature, $\beta = 7.1$, is chosen for the equilibrium system. In the strong-coupling regime considered in this Letter, this additional scattering channel can be partially attributed to a *repulsive* superexchange interaction for neighboring electronlike and holelike quasiparticles [25,49]. The analogous behavior is seen for the electron-doped side [Fig. 3(b)], where we compare the upper Hubbard band region in the transient state and in an electron-doped system with filling $n = 1 + n_e$.

Another useful comparison between chemically doped and photodoped states can be made for the optical conductivity $\sigma(\omega)$; see Fig. 3(c). (The optical conductivity is evaluated as in Ref. [25] and the Supplemental Material [43].) We mainly focus on the low-frequency Drude peak. The mutual influence of electron and hole carriers becomes evident because adding up the conductivities $\sigma_e + \sigma_h$ of an electron-doped system at $n = 1 + n_e$ and a hole-doped system at $n = 1 - n_h$ ($\beta = 13$) overestimates the Drude contribution. This observation is in line with the fact that the presence of holes (electrons) reduces the conductivity of electrons (holes) by providing additional scattering. Instead, the Drude peak is well reproduced by the Drude peak of a chemically doped system with filling $n = 1 + n_e + n_h$ and inverse temperature $\tilde{\beta}$, similar to the half-filled case [50].

Finally, we comment on the relaxation dynamics. The effective temperature $\tilde{T} = 1/\tilde{\beta}$ of the transient state is plotted as a function of time in Fig. 4(a) for different values of $\delta$. After the quench, $\tilde{T}$ decreases rapidly, as energy is transferred to the bath. At $t \gtrsim 300$, after the appearance of the quasiparticle peak, the dynamics slows down and $\tilde{T}$ relaxes with a roughly constant rate towards the bath temperature $T_f$. This slowdown of the relaxation, which becomes more pronounced in the underdoped regime [Fig. 4(b)], is a rather striking result. Possible explanations based on phase-space arguments and the bath density of states (such as a phonon bottleneck [51]) are unlikely because a simulation of the same dynamics in the weak-$U$ metallic regime, with the same bath coupling $\lambda$ and bath density of states, shows a rapid cooling of the electrons at a fast rate until the temperature $T_f$ is reached up to the numerical accuracy (see the curve labeled $U = 2$, which has been obtained with nonequilibrium DMFT and a second-order self-energy). The inefficient transfer of energy from the correlated electron liquid to the phonons is reminiscent of what has been observed in heavy fermion systems [52], although in the present case the system is not yet a Fermi liquid, and an understanding in terms of a kinetic picture is therefore naturally difficult. At present, we have no analytical understanding for this numerical prediction, but it should be observable by monitoring the evolution of the distribution function in photoemission spectroscopy, and it has the rather profound consequence that good metallic Fermi-liquid states are hard to reach by photodoping, even in clean systems without trapping of charge carriers by impurities or in polaronic and excitonic states.

*Conclusion.* In summary, we studied the long-time dynamics of photodoped Mott insulators coupled to a thermal reservoir. By photodoping an initially doped system, one can generate a strange metal with unequal densities of electronlike and holelike carriers. The following aspects may be of interest to future studies and experiments: (i) We find that the photodoped conductivity is in agreement with the conductivity of the chemically doped system, as observed in Ref. [15]. (ii) Holes and electrons do have different spectral properties. It will be interesting to see whether this behavior has an influence on the heat and charge transport. An intriguing experiment which would be within reach would be a diffusion measurement in a cold atom setting [53,54]. (iii) Finally, one remarkable finding is the extremely slow energy relaxation in the resilient quasiparticle regime. On the timescales of the simulation (2000 hopping times $\hbar/J$, corresponding to 5 picoseconds if the bandwidth is $4J = 1$ eV), the effective temperature of the system remains in the range where the equilibrium system would be in the resilient quasiparticle regime. As a consequence of the slow relaxation, even on the ps timescale, it is difficult to turn a photodoped Mott insulator into a good metal. Alternative routes may be cooling by photodoping protocols [50]. Our theoretical prediction of slow energy relaxation can be measured experimentally using cuprates and organic charge-transfer salts. In real materials, a possible interesting effect not captured by the present setting is the appearance of excitonic states. However, in Mott insulators, such bound states are expected to exist mainly in the tightly bound limit, which requires a rather strong nonlocal Coulomb interaction [55].

*Acknowledgments.* This work was supported by the ERC Starting Grant No. 716648. The calculations have been done at the RRZE of the University Erlangen-Nuremberg. P.W. acknowledges support from ERC Consolidator Grant No. 724103.

[1] C. Giannetti, M. Capone, D. Fausti, M. Fabrizio, F. Parmigiani, and D. Mihailovic, Adv. Phys. **65**, 58 (2016).

[2] D. N. Basov, R. D. Averitt, and D. Hsieh, Nat. Mater. **16**, 1077 (2017).

[3] D. Fausti, R. I. Tobey, N. Dean, S. Kaiser, A. Dienst, M. C. Hoffmann, S. Pyon, T. Takayama, H. Takagi, and A. Cavalleri, Science **331**, 189 (2011).

[4] S. Kaiser, C. R. Hunt, D. Nicoletti, W. Hu, I. Gierz, H. Y. Liu, M. Le Tacon, T. Loew, D. Haug, B. Keimer, and A. Cavalleri, Phys. Rev. B **89**, 184516 (2014).

[5] L. Stojchevska, I. Vaskivskyi, T. Mertelj, P. Kusar, D. Svetin, S. Brazovskii, and D. Mihailovic, Science **344**, 177 (2014).

[6] M. Mitrano, A. Cantaluppi, D. Nicoletti, S. Kaiser, A. Perucchi, S. Lupi, P. Di Pietro, D. Pontiroli, M. Riccò, S. R. Clark *et al.*, Nature (London) **530**, 461 (2016).

[7] P. A. Lee, N. Nagaosa, and X.-G. Wen, Rev. Mod. Phys. **78**, 17 (2006).

[8] S. Iwai, M. Ono, A. Maeda, H. Matsuzaki, H. Kishida, H. Okamoto, and Y. Tokura, Phys. Rev. Lett. **91**, 057401 (2003).

[9] S. Wall, D. Brida, S. R. Clark, H. P. Ehrke, D. Jaksch, A. Ardavan, S. Bonora, H. Uemura, Y. Takahashi, T. Hasegawa, H. Okamoto, G. Cerullo, and A. Cavalleri, Nat. Phys. **7**, 114 (2011).

[10] H. Okamoto, H. Matsuzaki, T. Wakabayashi, Y. Takahashi, and T. Hasegawa, Phys. Rev. Lett. **98**, 037401 (2007).

[11] H. Okamoto, T. Miyagoe, K. Kobayashi, H. Uemura, H. Nishioka, H. Matsuzaki, A. Sawa, and Y. Tokura, Phys. Rev. B **82**, 060513(R) (2010).

[12] H. Okamoto, T. Miyagoe, K. Kobayashi, H. Uemura, H. Nishioka, H. Matsuzaki, A. Sawa, and Y. Tokura, Phys. Rev. B **83**, 125102 (2011).

[13] M. Mitrano, G. Cotugno, S. R. Clark, R. Singla, S. Kaiser, J. Stähler, R. Beyer, M. Dressel, L. Baldassarre, D. Nicoletti, A. Perucchi, T. Hasegawa, H. Okamoto, D. Jaksch, and A. Cavalleri, Phys. Rev. Lett. **112**, 117801 (2014).

[14] T. Miyamoto, Y. Matsui, T. Terashige, T. Morimoto, N. Sono, H. Yada, S. Ishihara, Y. Watanabe, S. Adachi, T. Ito, K. Oka, A. Sawa, and H. Okamoto, Nat. Commun. **9**, 3948 (2018).

[15] J. C. Petersen, A. Farahani, D. G. Sahota, R. Liang, and J. S. Dodge, Phys. Rev. B **96**, 115133 (2017).

[16] D. G. Sahota, R. Liang, M. Dion, P. Fournier, H. A. Dabkowska, G. M. Luke, and J. S. Dodge, Phys. Rev. Res. **1**, 033214 (2019).

[17] N. Strohmaier, D. Greif, R. Jördens, L. Tarruell, H. Moritz, T. Esslinger, R. Sensarma, D. Pekker, E. Altman, and E. Demler, Phys. Rev. Lett. **104**, 080401 (2010).

[18] R. Sensarma, D. Pekker, E. Altman, E. Demler, N. Strohmaier, D. Greif, R. Jördens, L. Tarruell, H. Moritz, and T. Esslinger, Phys. Rev. B **82**, 224302 (2010).

[19] Z. Lenarčič and P. Prelovšek, Phys. Rev. Lett. **111**, 016401 (2013).

[20] Z. Lenarčič and P. Prelovšek, Phys. Rev. B **90**, 235136 (2014).

[21] Z. Lenarčič, M. Eckstein, and P. Prelovšek, Phys. Rev. B **92**, 201104(R) (2015).

[22] M. Eckstein and P. Werner, Phys. Rev. B **84**, 035122 (2011).

[23] A. Rosch, D. Rasch, B. Binz, and M. Vojta, Phys. Rev. Lett. **101**, 265301 (2008).

[24] F. Peronaci, O. Parcollet, and M. Schiró, Phys. Rev. B **101**, 161101(R) (2020).

[25] J. Li, D. Golez, P. Werner, and M. Eckstein, Phys. Rev. B **102**, 165136 (2020).

[26] X. Deng, J. Mravlje, R. Žitko, M. Ferrero, G. Kotliar, and A. Georges, Phys. Rev. Lett. **110**, 086401 (2013).

[27] A. Georges, L. d. Medici, and J. Mravlje, Annu. Rev. Condens. Matter Phys. **4**, 137 (2013).

[28] Y. Wang, Y. He, K. Wohlfeld, M. Hashimoto, E. W. Huang, D. Lu, S.-K. Mo, S. Komiya, C. Jia, B. Moritz *et al.*, Commun. Phys. **3**, 210 (2020).

[29] A. Legros, S. Benhabib, W. Tabis, F. Laliberté, M. Dion, M. Lizaire, B. Vignolle, D. Vignolles, H. Raffy, Z. Z. Li, P. Auban-Senzier, N. Doiron-Leyraud, P. Fournier, D. Colson, L. Taillefer, and C. Proust, Nat. Phys. **15**, 142 (2019).

[30] R. Daou, N. Doiron-Leyraud, D. LeBoeuf, S. Y. Li, F. Laliberté, O. Cyr-Choinière, Y. J. Jo, L. Balicas, J. Q. Yan, J. S. Zhou, J. B. Goodenough, and L. Taillefer, Nat. Phys. **5**, 31 (2009).

[31] P. Werner, E. Gull, M. Troyer, and A. J. Millis, Phys. Rev. Lett. **101**, 166405 (2008).

[32] O. Parcollet and A. Georges, Phys. Rev. B **59**, 5341 (1999).

[33] J. Vučičević, D. Tanasković, M. J. Rozenberg, and V. Dobrosavljević, Phys. Rev. Lett. **114**, 246402 (2015).

[34] N. Pakhira and R. H. McKenzie, Phys. Rev. B **91**, 075124 (2015).

[35] M. Eckstein and P. Werner, Phys. Rev. Lett. **110**, 126401 (2013).

[36] S. Sayyad and M. Eckstein, Phys. Rev. Lett. **117**, 096403 (2016).

[37] A. Georges, G. Kotliar, W. Krauth, and M. J. Rozenberg, Rev. Mod. Phys. **68**, 13 (1996).

[38] M. Schüler, M. Eckstein, and P. Werner, Phys. Rev. B **97**, 245129 (2018).

[39] M. Schüler, D. Golež, Y. Murakami, N. Bittner, A. Herrmann, H. U. Strand, P. Werner, and M. Eckstein, Comput. Phys. Commun. **257**, 107484 (2020).

[40] C. Stahl, D. Nagamalleswararao, P. Antonio, J. Li, and M. Eckstein, Memory truncated Kadanoff-Baym equations (unpublished).

[41] H. Aoki, N. Tsuji, M. Eckstein, M. Kollar, T. Oka, and P. Werner, Rev. Mod. Phys. **86**, 779 (2014).

[42] M. Eckstein and P. Werner, Phys. Rev. B **82**, 115115 (2010).

[43] See Supplemental Material at http://link.aps.org/supplemental/10.1103/PhysRevB.103.L201116 for the details of the memory truncation scheme, pulse driven dynamics, and optical conductivity.

[44] J. Li and M. Eckstein, Phys. Rev. B **103**, 045133 (2021).

[45] S.-S. B. Lee, J. von Delft, and A. Weichselbaum, Phys. Rev. Lett. **119**, 236402 (2017).

[46] S. B. Dugdale, Phys. Scr. **91**, 053009 (2016).

[47] G. Baym and C. Pethick, in *Landau Fermi-Liquid Theory* (Wiley, New York, 2007), Chap. 1, pp. 1–121.

[48] K. Byczuk, M. Kollar, K. Held, Y.-F. Yang, I. Nekrasov, T. Pruschke, and D. Vollhardt, Nat. Phys. **3**, 168 (2007).

[49] The interaction has the form of $-J_{\mathrm{ex}}(n_i - 1/2)(n_j - 1/2)$ with $J_{\mathrm{ex}} = 4J^2/U$. Starting with neighboring doubly occupied (electronlike) and empty (holelike) lattice sites, the interaction emerges due to a virtual process forming a virtual intermediate state of two singly occupied sites. The interaction is repulsive since the intermediate state has lower energy $(-U)$ than the initial and final real states.

[50] P. Werner, J. Li, D. Golež, and M. Eckstein, Phys. Rev. B **100**, 155130 (2019).

[51] J. D. Rameau, S. Freutel, A. F. Kemper, M. A. Sentef, J. K. Freericks, I. Avigo, M. Ligges, L. Rettig, Y. Yoshida, H. Eisaki, J. Schneeloch, R. D. Zhong, Z. J. Xu, G. D. Gu, P. D. Johnson, and U. Bovensiepen, Nat. Commun. **7**, 13761 (2016).

[52] J. Demsar, R. D. Averitt, K. H. Ahn, M. J. Graf, S. A. Trugman, V. V. Kabanov, J. L. Sarrao, and A. J. Taylor, Phys. Rev. Lett. **91**, 027401 (2003).

[53] P. T. Brown, D. Mitra, E. Guardado-Sanchez, R. Nourafkan, A. Reymbaut, C.-D. Hébert, S. Bergeron, A.-M. S. Tremblay, J. Kokalj, D. A. Huse, P. Schauß, and W. S. Bakr, Science **363**, 379 (2019).

[54] W. Xu, W. R. McGehee, W. N. Morong, and B. DeMarco, Nat. Commun. **10**, 1588 (2019).

[55] N. Bittner, D. Golež, M. Eckstein, and P. Werner, Phys. Rev. B **101**, 085127 (2020).